JOURNAL OF AIRCRAFT
Vol. 38, No. 3, May–June 2001

Engineering Notes

ENGINEERING NOTES are short manuscripts describing new developments or important results of a preliminary nature. These Notes cannot exceed 6 manuscript pages and 3 figures; a page of text may be substituted for a figure and vice versa. After informal review by the editors, they may be published within a few months of the date of receipt. Style requirements are the same as for regular contributions (see inside back cover).

Physical Analysis and Scaling of a Jet and Vortex Actuator

Jason T. Lachowicz*
National Research Council/NASA, Hampton, Virginia 23681
and
Chung-Sheng Yao† and Ronald D. Joslin‡
NASA Langley Research Center, Hampton, Virginia 23681

Nomenclature

a_d	=	actuator plate peak-to-peak displacement
b	=	actuator plate width, mm
d_y	=	estimated core vortex size, mm
dT	=	downward period of actuator plate, s; $1/(2^* f_{\text{rep}})$ for sine wave plate driver
f_{rep}	=	actuator plate driver pulse repetition rate, Hz
g_w	=	ratio of wide-slot width to (actuator) plate width, w_w/b
Re	=	Reynolds number, $\pi a_d b/2dT\nu$
S_a	=	scaled amplitude, $\pi a_d/b$
U	=	velocity component measured in the x direction (horizontal), m/s
w_w	=	wide-slot width, mm
x	=	distance along the width of the actuator plate measured from the edge of the wide slot
y	=	distance perpendicular to the actuator plate

Introduction

A PRIMARY goal of active flow control is to develop efficient actuators and sensors that can be integrated with flight-control systems to enhance aircraft performance at a reduced cost. Most of the research has focused on surface-mounted actuators that either reduce drag, enhance lift, or produce a controlled force about some axis of the aircraft. Unlike passive devices, which are typically optimized for a single flight condition, active control devices[1–3] produce no parasitic drag and can be effectively used for multiple flight conditions. Zero-net mass-flux actuators[1,2] are especially attractive because they require no internal ducts or pumps. This has the potential to significantly reduce the mass of the control system (hence the vehicle) and decrease the aircraft signature. The jet and vortex actuator (JaVA)[4,5] is a variant of a zero-net mass-flux actuator. Compared with other zero-net mass-flux actuators (e.g., a synthetic jet actuator[2]), the mechanisms of generating vorticity are different. Although a singular synthetic jet generates two symmetric vortices of opposite sense of rotation, the JaVA generates a single stationary vortex.

The JaVA consists of a cavity and rigid plate that is actuated uniformly into and out of a cavity using a mechanical oscillator. The plate acts like a piston pumping air out of the cavity on the downstroke and sucking air into the cavity on the upstroke. Following the work of Jacobson and Reynolds,[6] the plate is placed asymmetrically over the cavity opening, forming narrow and wide slots along the length of the plate surface (refer to Fig. 1 of Ref. 5).

In recent studies Lachowicz et al.[4,5] characterized the stand-alone JaVA driven by sine-wave forcing and found that several flowfields (wall jet, free jet, and vortex flow) were produced by the actuator. These flows were found to depend on Reynolds number, scaled amplitude, and g_w. Over the range of parameters surveyed in these studies, the maximum x-component velocity occurred at a Stokes number of approximately 7.9 for the vortex flow, and the core vortex was approximately 35% of the plate width.

The objectives of this Note are to study the JaVA-induced vortex flow using both sine and asymmetric plate forcing and to determine the nondimensional scaling of the actuator for the wall jet, free jet, and vortex flows. Variations in actuator geometry are also studied.

Approach

The experimental configuration of the JaVA is discussed in detail in Lachowicz et al.[5] All previously published results for the JaVA used sine-wave forcing to drive the actuator plate. Based on experimental observations and a theoretical analysis of the actuator flow physics, it is postulated that a form of asymmetric forcing is required to obtain a stronger induced vortex because the vortex-generation mechanism relies primarily on the downward stroke of the actuator plate motion. For asymmetric forcing the actuator plate is driven with a positive stroke that is different from the negative stroke and with a duration that is different from the duration for the negative stroke. Note that sine-wave forcing has equal duration and amplitude on both the positive and negative strokes. Various asymmetric forcing functions were initially studied. However, only results using a pulsed wave train are compared to sine-wave forcing in this study. (Hereafter, pulsed wave train forcing is referred to as asymmetric forcing.)

The nondimensional scaling and maximum mean vorticity were determined using flow visualization, actuator displacement measurements, and Laser Velocimetry. The experimental setup for these measurements is outlined in Ref. 5. A digital Particle Image Velocimetry (PIV) system was used to measure the instantaneous flow field in the x-y plane perpendicular to the actuator plate surface. The flowfield measurement was phase locked to eight equally spaced phases of the actuator plate motion. Particle images were recorded using a digital camera (1×1 K pixels) with a 105-mm lens. The spatial resolution of the measurement volume was less than 1 mm at the test plane. Ten samples of PIV images were taken at each phase.

Received 19 May 1999; revision received 29 June 2000; accepted for publication 8 September 2000.

*Research Associate; currently Department Chair of Automated Manufacturing Technology, ITT Technical Institute, Norfolk, VA.
†Senior Research Scientist, Fluid Mechanics and Acoustics Division.
‡Senior Research Scientist; currently Senior Research Associate, Applied Research Lab/Pennsylvania State University, State College, PA.

Ensemble averages were used to compute the phase-averaged flowfield.

Results

The actuator maximum mean vorticity, over a range of plate and wide-slot widths, is presented in Fig. 1. The maximum mean vorticity was estimated as $2^*(U_{\max} + |U_{\min}|)/d_y$, where d_y is the y distance between velocity maxima $U_{\min}$ and $U_{\max}$. (Refer to Ref. 5, Fig. 12, for a typical velocity profile of U vs y). The asymmetric driver is represented by the $w_w = 0.96$ mm, $b = 9.85$-mm case; all other cases use the sine-wave driver. Generally, the vorticity increases with repetition rate for both drivers at a fixed w_w and b. Assuming an extrapolation of the data is valid; the present data indicate that large potential gains in vorticity can be obtained using an asymmetric driver. For example, asymmetric forcing is compared to sine forcing at $f_{\text{rep}} = 130$ Hz at approximately the same wide-slot and plate width (observe open triangle and x symbols). At this repetition rate the vorticity is approximately 75% for the asymmetric driver. Additional measurements are needed at higher repetition rates to verify this trend at higher frequencies.

Figure 1 also illustrates the dependency of the maximum mean vorticity on plate width. For $f_{\text{rep}} < 125$ Hz (limit of data available for $b = 5.56$ mm) the vorticity is much larger for the smallest plate width relative to the larger plate widths considered. For example, for $g_w = w_w/b \approx 0.17$ (plus and square symbols) the vorticity for the $b = 5.56$-mm case is approximately 110% larger than the $b = 9.65$-mm case at a given repetition rate. But, the estimated core vortex size decreases by only 15% from $b = 9.65$ to 5.56 mm. Therefore, as plate width decreases a large increase in the vortex strength accompanies only a marginal decrease in the core size. The same trend occurs for $g_w \approx 0.10$ at $b = 5.56$ (filled circle) and 9.65 mm (open triangle). Hence, for a fixed g_w and repetition rate the vortex strength increases as the plate width decreases with only a relatively small decrease in core vortex size.

Using the same dimensional analysis outlined in Ref. 4, the nondimensional parameters were derived for the more general case of asymmetric forcing. These parameters are ($Re = \pi a_d b/2\,\mathrm{d}T\nu$, $S_a = \pi\, a_d/b$, and $g_w = w_w/b$) and are valid for both sine and asymmetric forcing. The general relationship between these parameters for both sine and asymmetric forcing is shown in Fig. 2 for the wall jet, free jet, and vortex flows. Although overlap exists between the flowfields, each flow has a region that is unique. Operation of the actuator in this unique region would produce the desired flow of interest. For example, at $Re\ g_w = 25$, $\sqrt{(Re/S_a)g_w^2} = 0.5$, the vortex flow exists; at $Re\, g_w = 25$, $\sqrt{(Re/S_a)g_w^2} = 1$, the

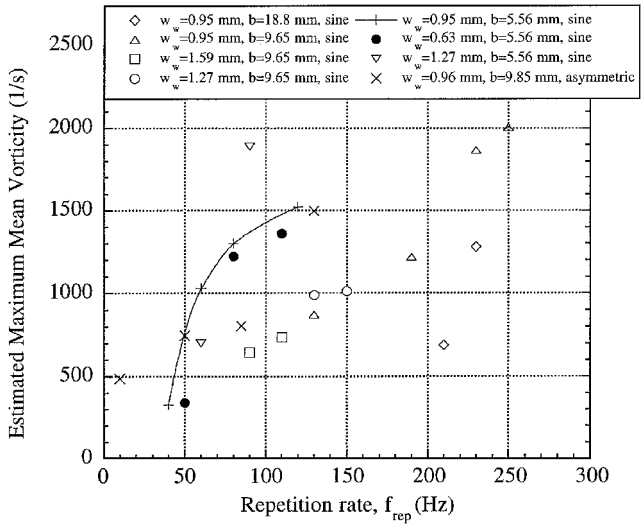

Fig. 1 Estimated maximum mean vorticity as a function of repetition rate.

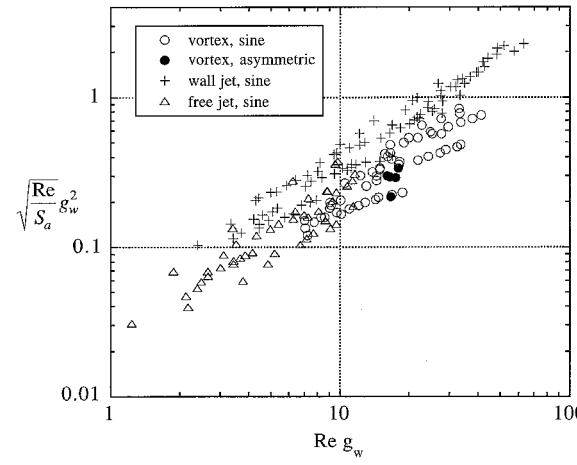

Fig. 2 Nondimensional scaling for JaVA.

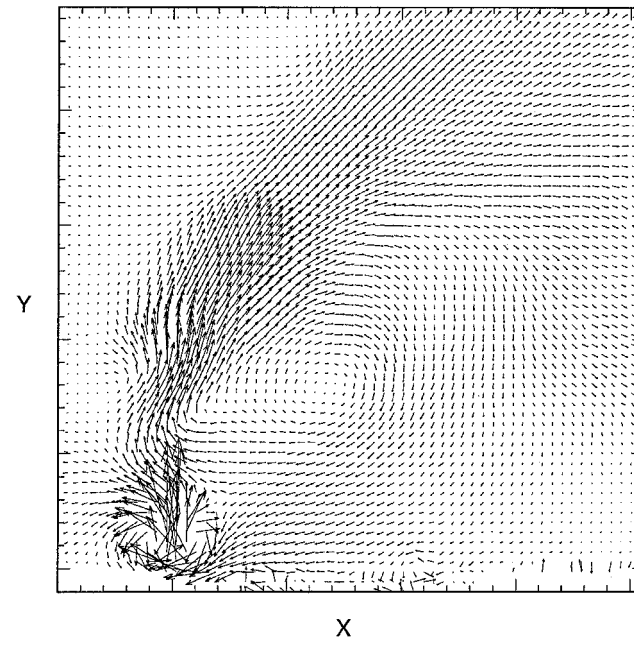

Fig. 3 Phase-averaged velocity field: phase 1 (plate into cavity).

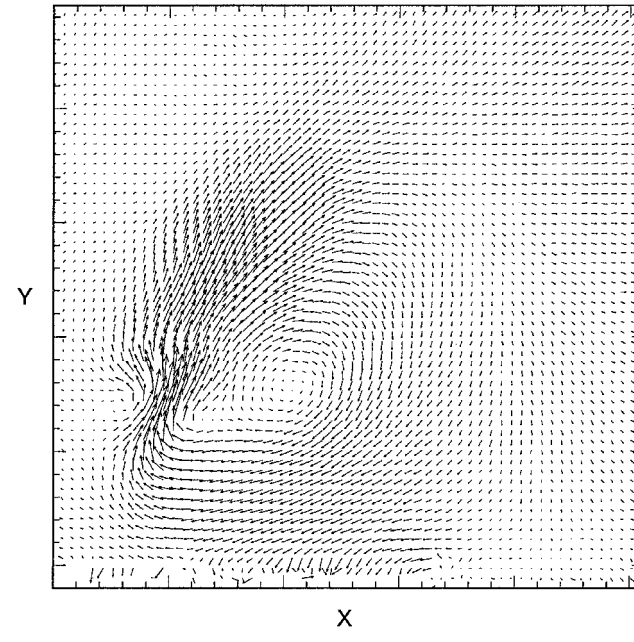

Fig. 4 Phase-averaged velocity field: phase 2 (plate out of cavity).

wall jet flow exists; and at $Re\, g_w = 4$, $\sqrt{(Re/S_a)}g_w^2 = 0.08$, the free jet exists. For the vortex flow the scaling region is approximately the same for both types of forcing, suggesting that the scaling is not dependent on the type of forcing used in this study.

Figures 3 and 4 depict the phase-averaged velocity fields for the actuator operating in the vortex mode. Each figure represents the average of 10 samples at a particular phase of the actuator plate oscillation. As seen, a vortex structure is measured above the piston for each phase suggesting that the structure is stationary; note that similar results are observed for the additional six phases not presented. This trend is consistent with the averaged flow-visualization pattern and computations.[7] In addition, an unsteady angled jet flow is pumped from the wide gap, which is indicative of mass ejection from the actuator. Each of the phase-averaged velocity fields were averaged to compute the mean flowfield. This result (not presented) indicates that a single cell vortex is generated from the actuator and also verifies the stationarity of the vortex.

Concluding Remarks

A parameter study of the stand-alone JaVA has been implemented for the vortex flowfield. The actuator plate size and forcing were varied to change the strength of the actuator-induced vortex. Measurements indicated that the vortex strength increases with driver repetition rate for a fixed wide slot and plate width. For a fixed driver repetition rate and wide-slot to plate-width ratio, the vortex strength increased as the plate width decreased with only a relatively small decrease in core vortex size. Using an asymmetric plate driver, a stronger vortex is generated for the same actuator geometry and driver repetition rate; however, this trend needs to be verified at higher frequencies. The phase-locked velocity measurements indicated that the vortex structure is stationary and (expectantly) shows unsteadiness near the wide-slot opening. Both of these results are consistent with earlier computations. The nondimensional scaling for the actuator was determined and provided an operating range for the actuator in different flow regimes. When placed in a turbulent boundary layer, the actuator (operated in the vortex regime) can potentially be used to generate streamwise vortices to control flow separation. When operated in the wall regime, the actuator could potentially be used to locally accelerate a boundary-layer flow.

Acknowledgments

This work was performed while the first author held a National Research Council Post-Doctoral Fellowship at NASA Langley Research Center. This work was supported by the Aircraft Morphing element of the NASA Airframe Systems Program Office and by the Air Force Office of Scientific Research.

References

[1]Wiltse, J. M., and Glezer, A., "Manipulation of Free Shear Flows Using Piezoelectric Actuators," *Journal of Fluid Mechanics*, Vol. 249, 1993, pp. 261–285.

[2]Amitay, M., Smith, B. L., and Glezer, A., "Aerodynamic Flow Control Using Synthetic Jet Technology," AIAA Paper 98-0208, Jan. 1998.

[3]Compton, D. A., and Johnston, J. P., "Streamwise Vortex Production by Pitched and Skewed Jets in a Turbulent Boundary Layer," *AIAA Journal*, Vol. 30, No. 3, 1992, pp. 640–647.

[4]Lachowicz, J. T., Yao, C., and Wlezien, R. W., "Scaling of an Oscillatory Flow Control Actuator," AIAA Paper 98-0330, Jan. 1998.

[5]Lachowicz, J. T., Yao, C., and Wlezien, R. W., "Flow Field Characterization of a Jet and Vortex Actuator," *Experiments in Fluids*, Vol. 26, 1999, pp. 12–20.

[6]Jacobson, S. A., and Reynolds, W. C., "Active Control of Streamwise Vortices and Streaks in Boundary Layers," *Journal of Fluid Mechanics*, Vol. 360, 1998, pp. 179–212.

[7]Joslin, R. D., Lachowicz, J. T., and Yao, C., "DNS of Flow Induced by a Multi-Flow Actuator," American Society of Mechanical Engineers, Paper FEDSM98-5302, June 1998.

Sensing Aircraft Icing Effects by Unsteady Flap Hinge-Moment Measurement

Holly M. Gurbacki* and Michael B. Bragg†
University of Illinois at Urbana–Champaign, Urbana, Illinois 61801

Introduction

ICE-INDUCED flow separation can lead to severe performance degradation and reduced aircraft control effectiveness. Trunov and Ingelman-Sundberg[1] demonstrated the effects of ice and roughness on the hinge moment of a tailplane. For the clean, no-ice case the hinge-moment coefficient C_h increased linearly with negative angle of attack until rising sharply at stall. The nonlinearity was the result of flow separation from the lower tailplane surface, where the control surface was abruptly sucked downward as a result of decreased pressure. With ice or roughness at the leading edge, the break in the linear curve occurred at a smaller, less negative angle, and the increase in C_h was less abrupt, eventually leveling out after tailplane stall. Separated flow over a control surface can also lead to reduced control effectiveness. This effect was known as far back as 1940 when Johnson[2] measured a 40% reduction in roll authority as a result of the presence of ice.

Problems such as the increased magnitude in hinge moment and the loss of control effectiveness may have led to a number of ice-related aircraft accidents.[3] It is suspected that the ATR-72 commuter aircraft flight 4184 that crashed on 31 October 1994 in Roselawn, Indiana, is one such example. Bragg[4] studied the effects of supercooled large droplets (SLD) icing conditions on aircraft control and speculated as to the cause of the ATR incident. An ice ridge located aft of the upper surface deicing boot can result from the presence of SLD in the atmosphere and can have a detrimental effect on the lateral control of the aircraft.

Although the pilot and crew may be conscious of the presence of ice on the aircraft, they may be completely unaware of the severity of the icing condition and its effects on aircraft performance and handling qualities. In an effort to identify an easily measurable quantity lying at the source of the ice-induced unsteady separated flowfield, the rms flap hinge-moment coefficient was examined. Experimental results showed that the time-dependent hinge-moment coefficient indicated unsteadiness in the flowfield while the airfoil lift coefficient was still in the linear range. As the angle of attack was increased, a significant increase in the parameter occurred, clearly distinguishing the simulated-iced airfoil from the clean airfoil. The initial change in the time-dependent parameter always took place before the nonlinearity in the steady-state hinge moment, which occurred before the flowfield completely separated. The unsteady hinge-moment coefficient proved to be a viable warning of imminent performance and control degradation. The purpose of this Note is to describe these results in more detail.

Results and Discussion

Experiments were performed in a conventional 3×4 ft (91.44×121.92 cm) indraft, open-return, low-turbulence wind tunnel. The airfoil model was an 18-in. (45.72 cm) chord modified NACA 23012

Received 29 November 2000; revision received 5 January 2001; accepted for publication 25 January 2001.

*Graduate Research Assistant, Department of Aeronautical and Astronautical Engineering, 306 Talbot Lab, 104 S. Wright Street.

†Professor and Head, Department of Aeronautical and Astronautical Engineering, 306 Talbot Lab, 104 S. Wright Street.